Science Advances
AAAS

advances.sciencemag.org/cgi/content/full/6/16/eaay8271/DC1

Supplementary Materials for

Ultraprecise single-molecule localization microscopy enables in situ distance measurements in intact cells

Simao Coelho, Jongho Baek, Matthew S. Graus, James M. Halstead, Philip R. Nicovich, Kristen Feher, Hetvi Gandhi, J. Justin Gooding, Katharina Gaus*

*Corresponding author. Email: k.gaus@unsw.edu.au

Published 17 April 2020, *Sci. Adv.* **6**, eaay8271 (2020)
DOI: 10.1126/sciadv.aay8271

This PDF file includes:

Figs. S1 to S10

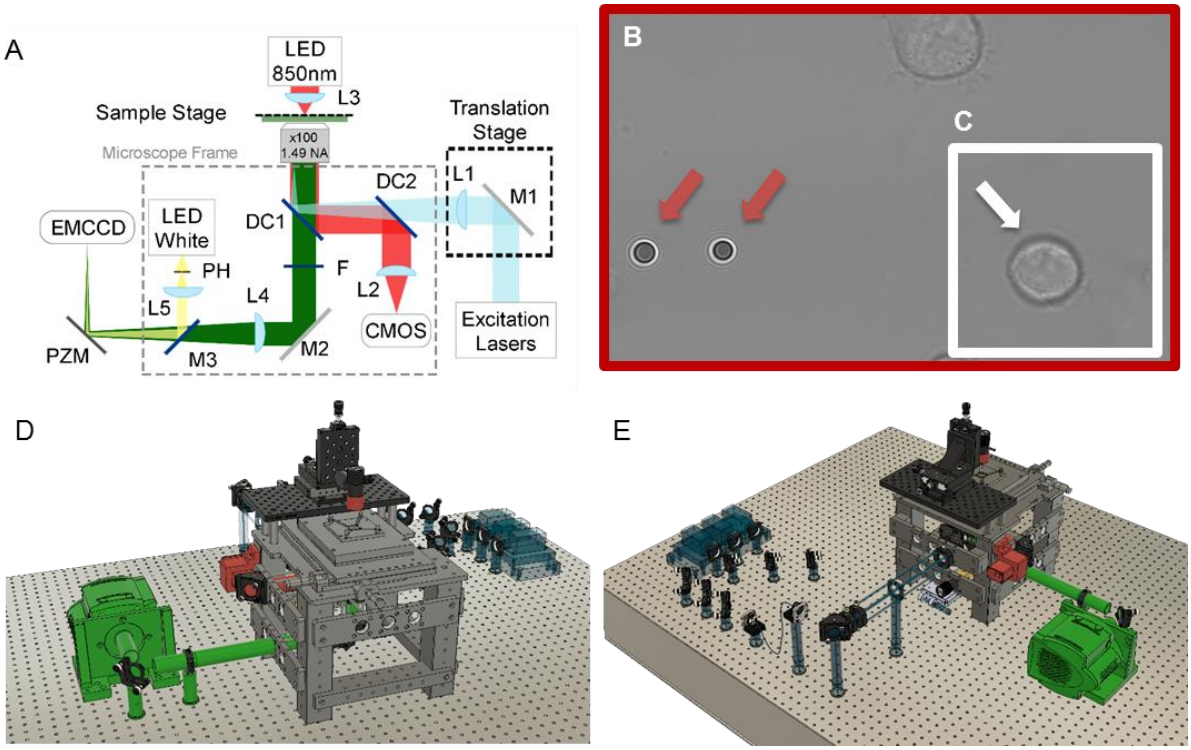

Fig. S1. Feedback SMLM setup. (A) Simplified design of the optical setup. Fluorescence, excited by lasers (light blue) under TIRF illumination (via a translation stage), is collected and imaged onto an EMCCD camera. A white LED (yellow) is combined with the emission light path and produces a reference point for the piezoelectric feedback correction. Sample drift is determined with 3 µm polystyrene fiducial beads in the sample, which are illuminated with an infrared LED and imaged with a dedicated CMOS camera. M1-2, mirrors; M3, 0.5% reflective mirror; L1-5, lenses; F, filter; DC1-2, dichroics; PZM, piezoelectric mirror; PH, pinhole; EMCCD, EMCCD camera. (B and C) Fields-of-views of the Feedback SMLM. Non-fluorescent fiducials were used outside the field of view (FoV) of the cameras for SMLM (white square). This provided great flexibility in sample positioning and ensured that fiducials did not interfere with data acquisition. (B) An infrared LED illuminated the sample and the polystyrene beads on the coverslip (red arrows). The beads created diffraction rings which were imaged with a CMOS camera with a FoV of 112 µm x 70 µm (red square). (C) FoV of the fluorescent EMCCD camera (40 µm x 40 µm). The white arrow points to a T cell in the FoV of the SMLM camera. The CMOS FoV is ~ 5 fold larger than the EMCCD camera. (D-E) CAD design of the Feedback SMLM. The highlighted color sections correspond to the excitation path (blue), the fluorescence path (green), the emission path stabilization (yellow) and sample stabilization path (red), as found in (A).

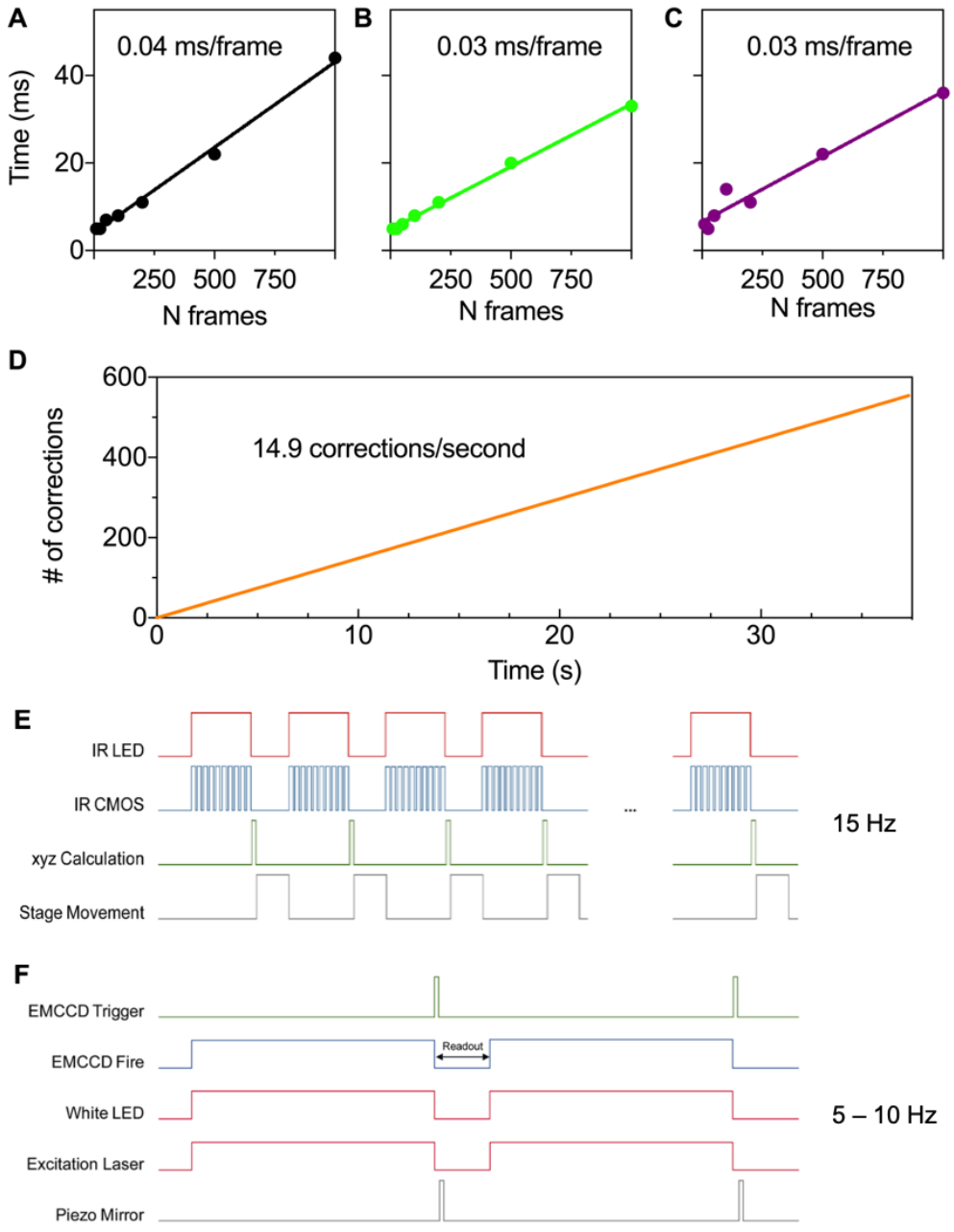

Fig. S2. Speed of GPU calculation, sample corrections and acquisition diagrams. (A-C), The 3D position of a simulated bead was calculated for a varying number of frames. (A) Processing time without pixel noise for a stationary bead. (B) Processing time without pixel noise for a mobile bead. (C) Processing time with pixel noise for a mobile bead. (D) Speed of stage correction. The number of sample corrections were recorded as a function of time. The slope of the line shows a frequency of 14.9 corrections per second. (E and F) Acquisition diagrams. (E) Diagram of the timing of sample stabilization during acquisition. The stage movement was synchronized with the acquisition of the CMOS camera. (F) Diagram of the timing of the fluorescence acquisition. To enhance acquisition speed, the piezo electric mirror was moved during the readout of the EMCCD.

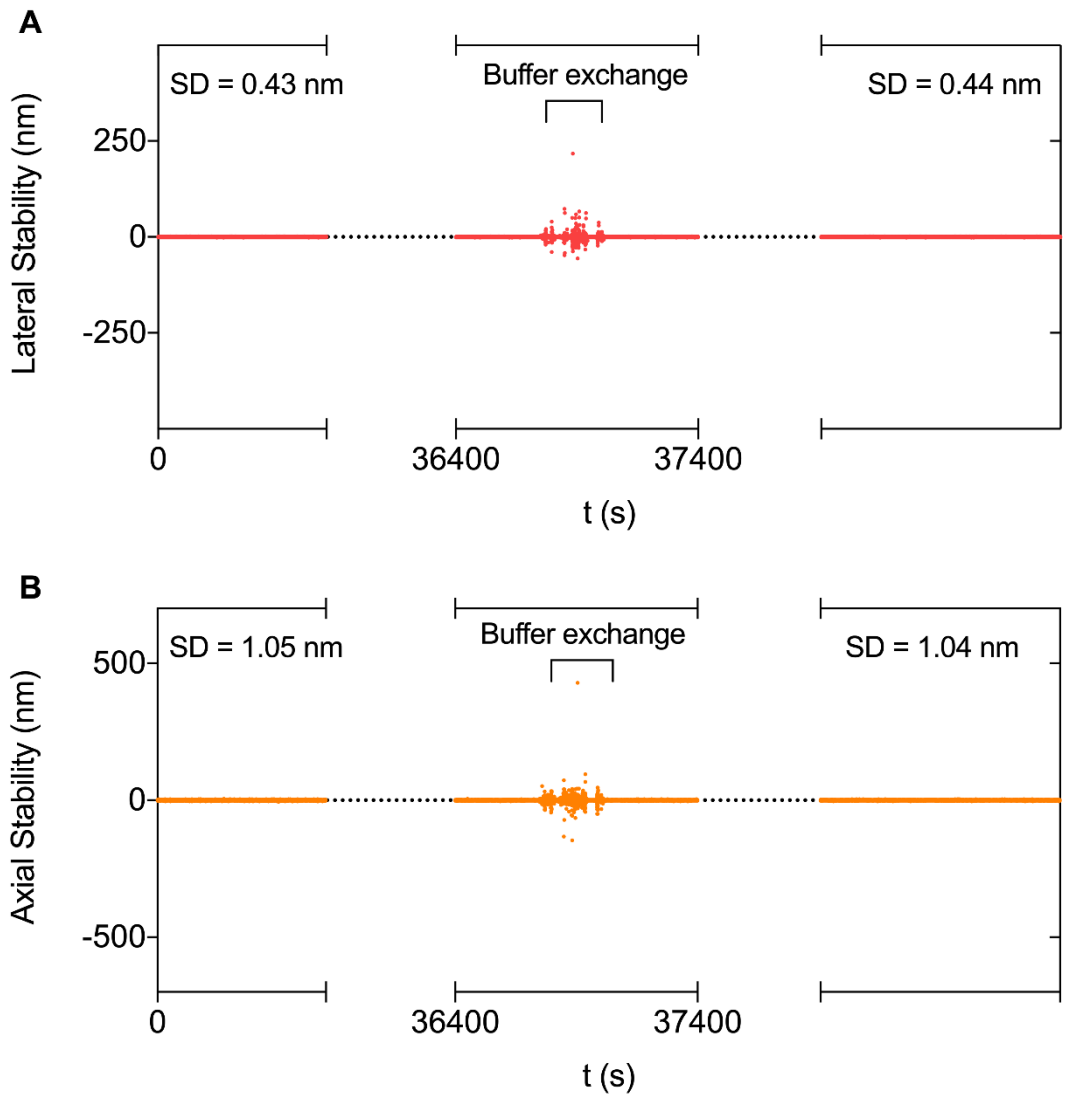

Fig. S3. Feedback SMLM corrects stage position during buffer exchanges. Beads were attached to a lipid bilayer and incubated overnight. A buffer exchange was performed which induced movement of the sample. The Feedback SMLM autonomously repositions the sample and corrects for drift introduced. (A) Lateral stabilization. Pre- and post-buffer exchange shows a standard deviation of 0.43 nm and 0.44 nm. (B) Axial stability. Pre- and post-buffer exchange shows a standard deviation of 1.05 nm and 1.04 nm.

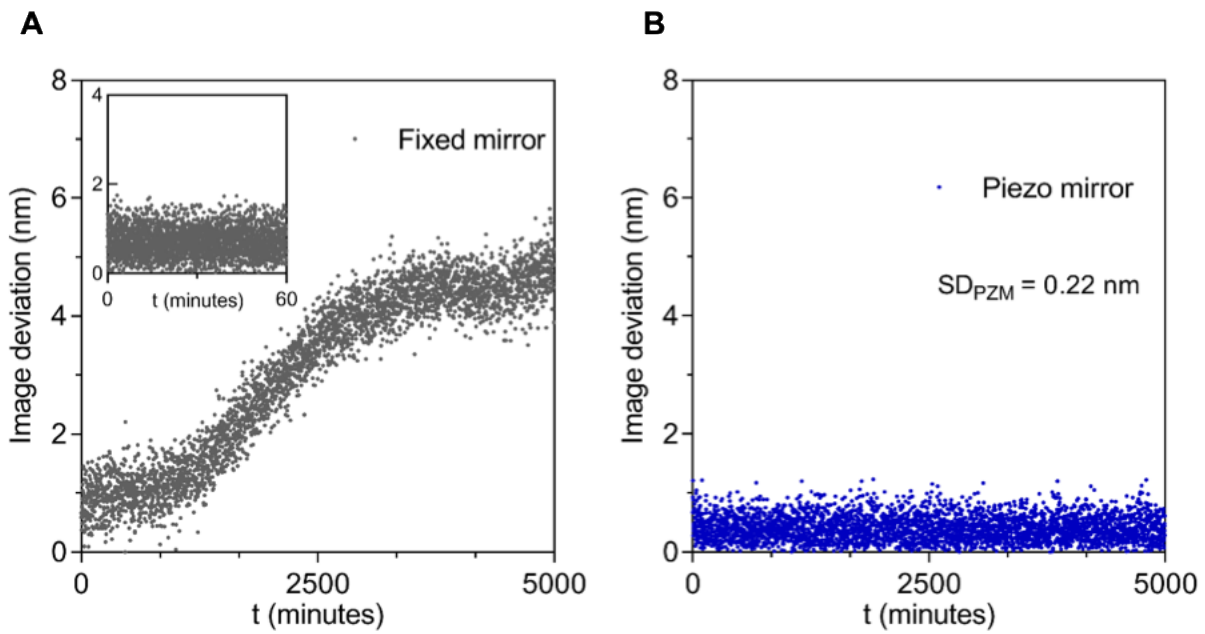

Fig. S4. Structural instability is detrimental to the fluorescence path. (A) Drift indicates slow movement of the structure over long periods of time. The piezo-electric mirror (PZM) (Fig. S1) was removed and replaced for a standard mirror. Image deviation was calculated as $(dx^2 + dy^2)^{0.5}$, where dx and dy represent deviations from the original set point of the LED (1/60 points plotted). Final image deviation is ~5 nm. Inset shows drift of the first 60 min and has a standard deviation 0.31 nm. Structural drift can be negligible for short-term imaging, however, must be accounted for in a prolonged acquisition (i.e. T cell multichannel PAINT imaging). (B) Stability of the microscope with the piezo-electric mirror is increased to 0.22 nm (1/120 points plotted). The piezo-electric mirror removes the need for any drift correction post-acquisition.

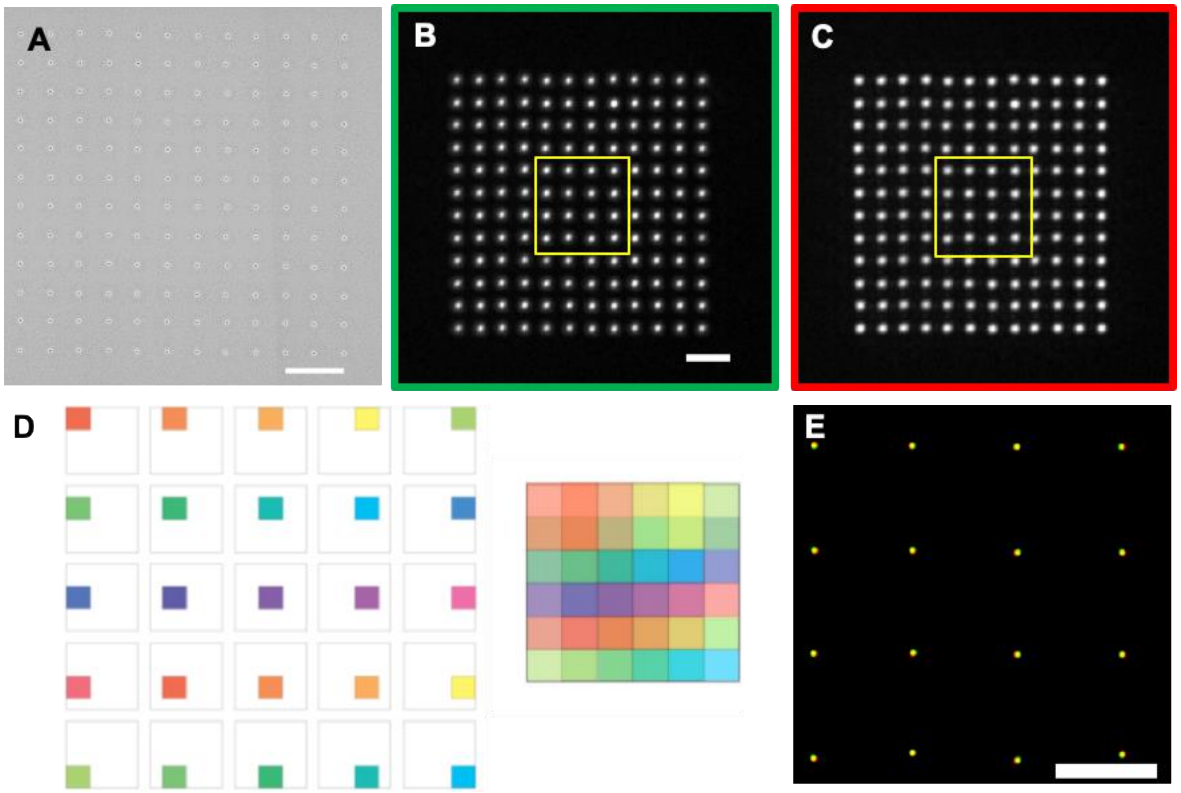

Fig. S5. EMCCD characterization and chromatic correction. The apparent variation between coordinates is due to the registration errors of the EMCCD, optical and chromatic aberrations. (A) Electron microscopy image of nanohole array used to test the EMCCD camera. The nanohole array consists of sub-diffraction-sized circular holes in an aluminum layer on a glass coverslip arranged in a regular grid pattern and separated by 1 µm. Scale bar = 2 µm. (B-C) The nanohole array was filled with green (Alexa488, B) red (Alexa647, C) dyes. Scale bar = 2 µm. (D) Graphical illustration of the camera testing procedure. The nanohole array which occupied 1/9 of the EMCCD area was stepped in discrete increments. Each step was equal to half the length of the nanohole array in both the horizontal and vertical directions. Stepping the sections over the entire space generated a final overlapped mask in which each overlapping segment contributes equally. (E) Residual errors after applying the correction was reduced ~10-fold. Localizations from the yellow square highlighted in (B) and (C) after EMCCD correction. Scale bar = 1 µm.

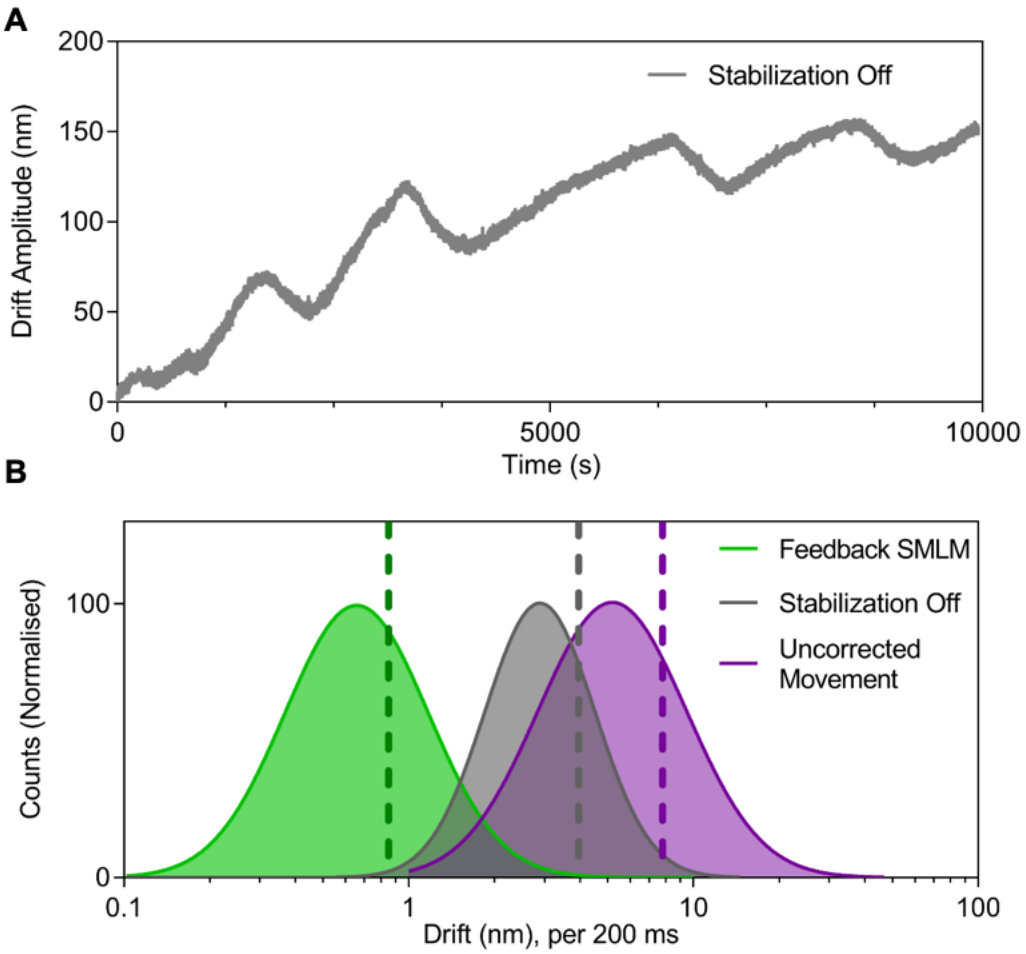

Fig. S6. Drift during fluorescence acquisition negatively affects the localization precision. The 3D position of a 3 µm bead was registered every 67 ms. (A) Sample drift without active stabilization. The drift amplitude (d) was calculated as $d = (dx^2 + dy^2 + dz^2)^{0.5}$, where dx, dy and dz represent deviations from the start point. The final drift amplitude after ~ 3 hours is 150 nm. The drift is small in comparison to a standard SMLM system. (B) Normalized drift histograms. Drift was calculated every 200 ms to match the binding time of a DNA-PAINT imaging strand. The mean displacement of the Feedback SMLM (green curve) is 0.84 nm (green dotted line). The mean displacement with the stabilization off (grey curve) is 3.54 nm (grey dotted line). Without stabilization, the uncorrected distance travelled (purple curve) within 200 ms is 5.7 nm (purple dotted line). The uncorrected distance was calculated as the total distance travelled after 200 ms.

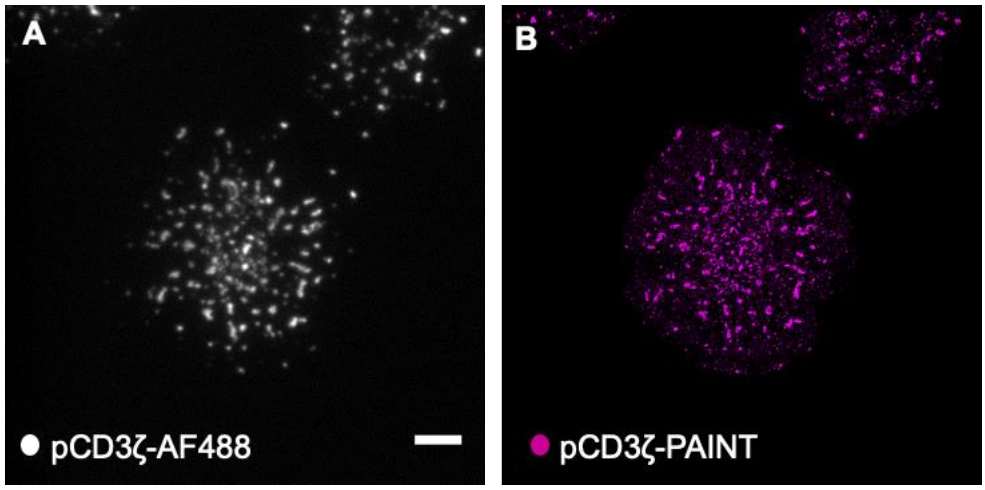

Fig. S7. T cell activation. (A) TIRF image of antibody-stained phosphorylated CD3ζ (pCD3ζ). The secondary antibody was conjugated to Alexa 488. (B) DNA-PAINT image of primary antibody pCD3ζ (magenta) shows high spatial correlation with (A). The primary and secondary antibody staining confirms spatial clustering of pCD3ζ and specificity of the DNA-PAINT. Scale bar = 4 μm.

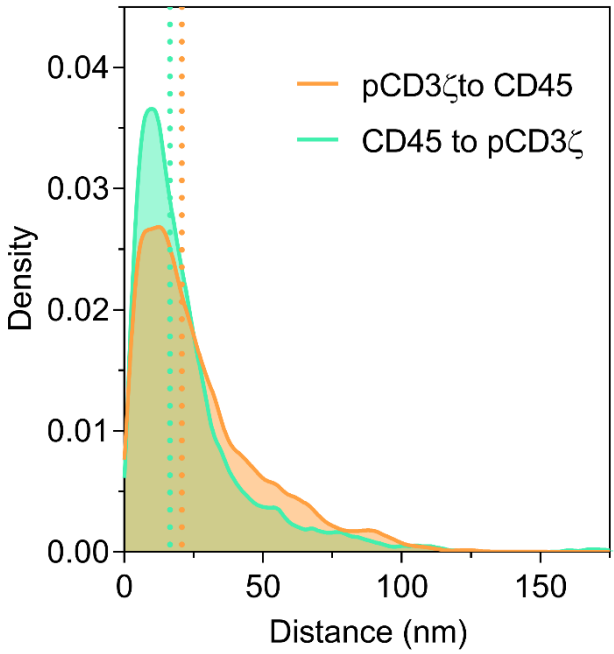

Fig. S8. Nearest neighbor distance analysis of combined regions of interest between CD45 and pCD3ζ in Jurkat cells. Nearest neighbor distances between CD45 (green) and pCD3ζ (orange) for 40 individual regions of interest (10 per cell) were pooled. The median distance of pCD3ζ to CD45 is 20.8 nm (orange dotted line). The median distance of CD45 to pCD3ζ is 16.5 nm (green dotted line).

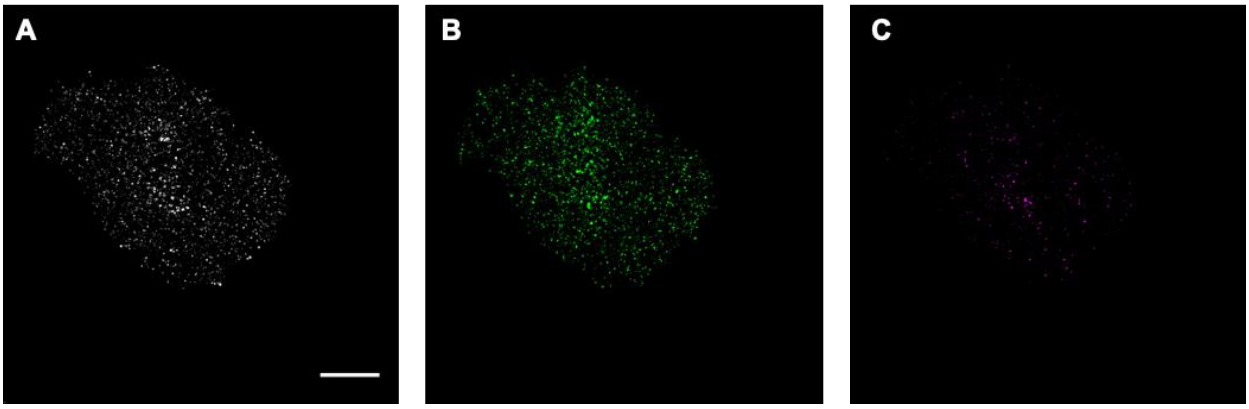

Fig. S9. Non-activated resting Jurkat cells. DNA-PAINT image of (A) CD3ε (white), (B) phosphorylated pCD3ζ (magenta) and (C) CD45 (green) in resting T cells. Scale bar = 6 µm.

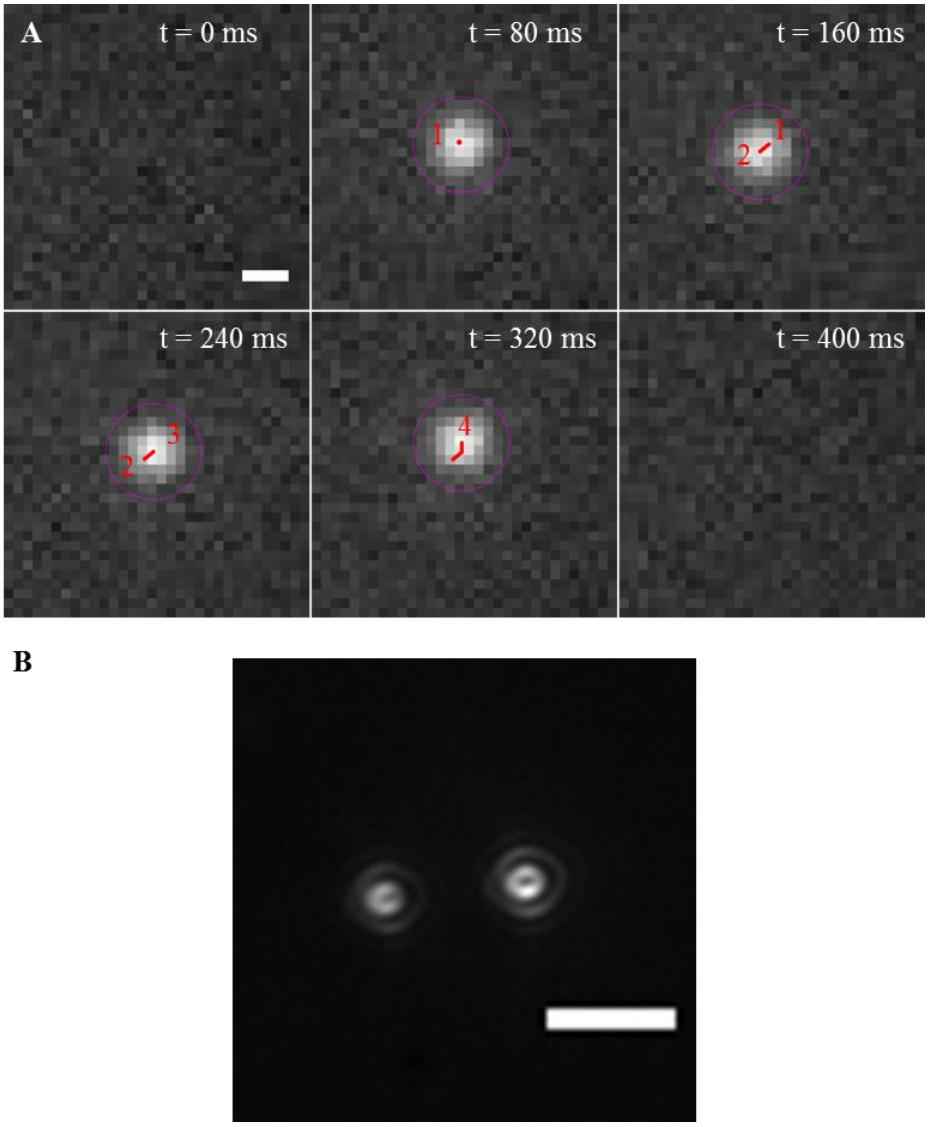

Fig. S10. Influence of lipid bilayers on DNA origami and gold nanorods fiducials. (A) DNA origami structures are laterally mobile on lipid bilayers. DNA origami structures were deposited on lipid bilayers and the movement (red line, 1-4) of individual binding events (purple circle) monitored over time. Feedback SMLM could clearly detect the lateral movement. The movement was not due to drift as the sample was stabilized with a standard deviation of 0.39 nm and 1.1 nm in the lateral and axial directions, respectively. Scale bar = 400 nm. (B) Gold nanorods can have orientation-dependent emission potentially impacting post-acquisition drift corrections. Gold nanorods were deposited on lipid bilayers and imaged. Once inserted into the bilayer, the emission profile detected is dependent on the orientation of the nanorod with respect to the laser. Typical post-acquisition drift correction software assumes fiducials are diffraction-limited Gaussian emitters and do not account for variations of the emission profile. The Feedback SMLM operates independently from the fluorescent acquisition and does not require post-acquisition correction. Scale bar = 2 µm.